PROCEEDINGS OF SCIENCE

Non-leptonic hadron decays at the LHC

R. Novotný, on behalf of the ATLAS, CMS and LHCb collaborations

Department of Physics and Astronomy, University of New Mexico, Albuquerque, NM, USA, 87131

E-mail: radek.novotny@cern.ch

This manuscript is devoted to the overview of the most recent measurements of non-leptonic hadron decays at the LHC, including results from the ATLAS, CMS, and LHCb collaborations. The non-leptonic hadron decays cover a very rich sample of the physics phenomena that form the foundation of the Standard Model of particle physics and could show effects from new particles that are not included in the Standard Model predictions. There exist multiple physics analyses of non-leptonic hadron decays, focusing on various aspects of these decays. Some of them focus on the search for rare decays that are constrained by theoretical predictions; others provide new precise measurements of known channels. Altogether, these measurements improve existing theories and bring us deeper understanding of these processes.

21st Conference on Flavor Physics and CP Violation (FPCP 2023)
29 May - 2 June 2023
Lyon, France

PoS(FPCP2023)004

1. Introduction

The Large Hadron Collider (LHC) [1] provided a sizeable sample of pp collisions at 13 TeV that were recorded between the years 2015 and 2018, denoted as LHC Run 2. This data sample contains a very rich content of non-leptonic hadron decays, and the increased production cross-section with respect to the 8 TeV energy allows the measurement of rare decays that were not previously accessible. It also provides sufficient statistics for increased precision measurements of previously known decays. This manuscript focuses on the most recent non-leptonic hadron decay measurements, including results from the ATLAS [2], CMS [3], and LHCb [4] collaborations.

2. Purely hadronic decays

The first group of analyses focuses on the differences in the way B mesons decay to baryonic versus purely mesonic final states. This differences are known from earlier measurements; however, a deep understanding of it is still missing. To date, only three charmless two-body baryonic decays have been observed, namely $B^+ \to p\bar{\Lambda}(1520)$, $B^+ \to p\bar{\Lambda}$ and $B^0 \to p\bar{p}$. These decays can go through factorizable W-exchange, non-factorizable internal W-emission, and penguin level gluon-exchange and annihilation diagrams. Many theories predict the branching ratio of the $B_s \to p\bar{p}$ decay to be vanishingly small; however, some of them allow a yield $\mathcal{B}(B_s^0 \to pp) \sim 10^{-8}$ that is experimentally accessible [6]. This is the reason why the study of this channel is important for understanding the role of exchange and annihilation diagrams in baryonic B decays.

LHCb performed a search for the rare hadronic decay $B_s^0 \to p\bar{p}$ using full Run 2 data with an integrated luminosity of 6 fb^{-1} [5]. This analysis also includes the measurements of $B^0 \to p\bar{p}$ decays. The $B^0 \to K^+\pi^-$ decay was used as the control channel for both measurements. The candidate selection is based on an initial set of selection criteria, which include requirements on particle identification, and is followed by a multivariate classifier relying on a boosted decision tree (BDT). The unbinned maximum likelihood fit was performed on the reconstructed $p\bar{p}$ invariant mass spectrum as shown in Figure 1.

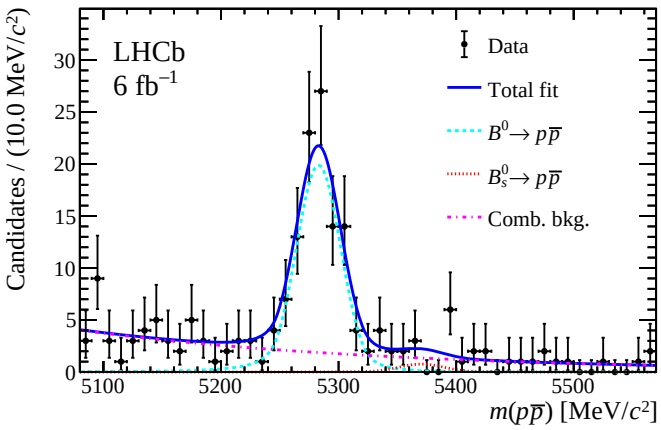

Figure 1: Invariant-mass distribution of $p\bar{p}$ candidates with each fit model component. Taken from [5].

The significances following Wilk's theorem [7] extracted from the fit to the $p\bar{p}$ data are 16.2σ and 0.9σ for the $B^0 \to p\bar{p}$ and $B_s^0 \to p\bar{p}$, respectively. The branching ratio of $B^0 \to p\bar{p}$ is measured to be $\mathcal{B}(B^0 \to p\bar{p}) = (1.27 \pm 0.15(\text{stat.}) \pm 0.05(\text{syst.}) \pm 0.04(\text{ext.})) \times 10^{-8}$, where the first uncertainty is statistical, the second is systematic and the third is due to the uncertainty on the branching fraction of the normalization channel. Since no significant evidence for $B_s^0 \to p\bar{p}$ was observed, the upper limit was set at $\mathcal{B}(B_s^0 \to p\bar{p}) < 4.4(5.1) \times 10^{-9}$ at 90% (95%) CL.

Another LHCb analysis focuses on the four-body decays of B mesons that are not as suppressed relative to the corresponding two-body decays. LHCb performed a search for $B^0 \to p\bar{p}p\bar{p}$ and $B_s^0 \to p\bar{p}p\bar{p}$ decays using a dataset with integrated luminosity of $9\,\text{fb}^{-1}$ combining LHC Run 1 and Run 2 samples [8]. Neither of fully baryonic decays $B^0 \to p\bar{p}p\bar{p}$ or the $B_s^0 \to p\bar{p}p\bar{p}$ have been observed previously. The search for these two decays was based on blinded analyses using two sets of cuts, tight and very tight, that were optimized for the B^0 and B_s^0, respectively. The unbinned maximum likelihood fit applied to the $p\bar{p}p\bar{p}$ invariant mass spectrum (Figure 2) reveals two peaks with significance of 9.3σ and 4.0σ, respectively.

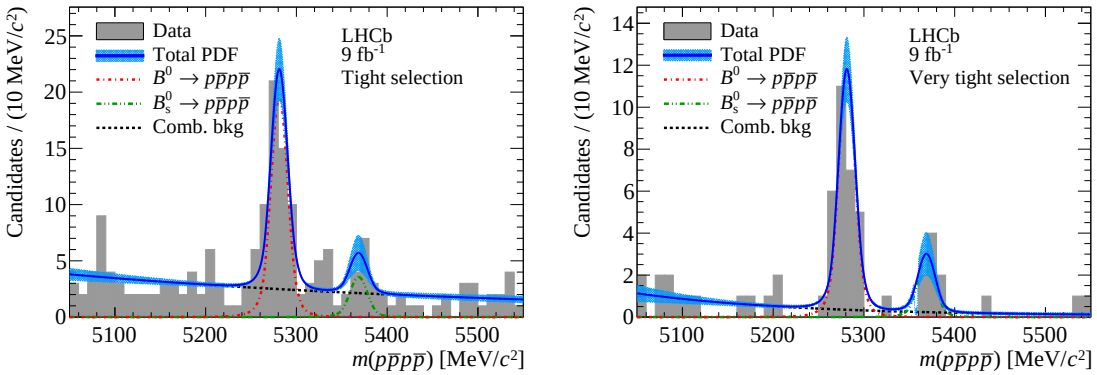

Figure 2: Invariant-mass distribution of $p\bar{p}p\bar{p}$ candidates with each fit model component for the tight (left) and very tight (right) selection cuts. Taken from [8].

The branching fractions were measured with respect to the normalization channels $B^0 \to J/\psi K^{*0}$ for $B^0 \to p\bar{p}p\bar{p}$ and $B_s^0 \to J/\psi\phi$ for $B_s^0 \to p\bar{p}p\bar{p}$. The resulting branching fractions are $B^0 \to p\bar{p}p\bar{p} = (2.2 \pm 0.4(\text{stat.}) \pm 0.1(\text{syst.}) \pm 0.1(\text{ext.})) \times 10^{-8}$ and $B_s^0 \to p\bar{p}p\bar{p} = (2.3 \pm 1.0(\text{stat.}) \pm 0.2(\text{syst.}) \pm 0.1(\text{ext.})) \times 10^{-8}$, where the first uncertainty is statistical, the second is systematic and the third is due to the external branching fraction of the normalization channel.

3. Analyses involving the B_c

The next group of analyses focuses on understanding the B_c properties. Operating LHC experiments at a center-of-mass energy $\sqrt{s} = 13\,\text{TeV}$ opens new opportunities to measure the properties of the B_c meson precisely. Previous studies were limited by the low B_c production cross-section. The first analysis involving the B_c meson mentioned here is from ATLAS where the $B_c^+ \to J/\psi D_s^+$ and $B_c^+ \to J/\psi D_s^{*+}$ decays were measured using full Run 2 data with an integrated luminosity of $139\,\text{fb}^{-1}$ [9]. The D_s^+ meson is reconstructed via the $D_s^+ \to \phi\pi^+$ decay, with the ϕ meson decaying into pairs of charged kaons. The D_s^{*+} meson decays into a D_s^+ meson

and a soft photon or π^0 which is not reconstructed in the analysis; however, the mass difference between the D_s^+ and D_s^{*+} is sufficient for the two decay signals to be resolved as two distinct structures in the reconstructed mass of the $J/\psi D_s^+$ system. Due to the fact that $B_c^+ \to J/\psi D_s^{*+}$

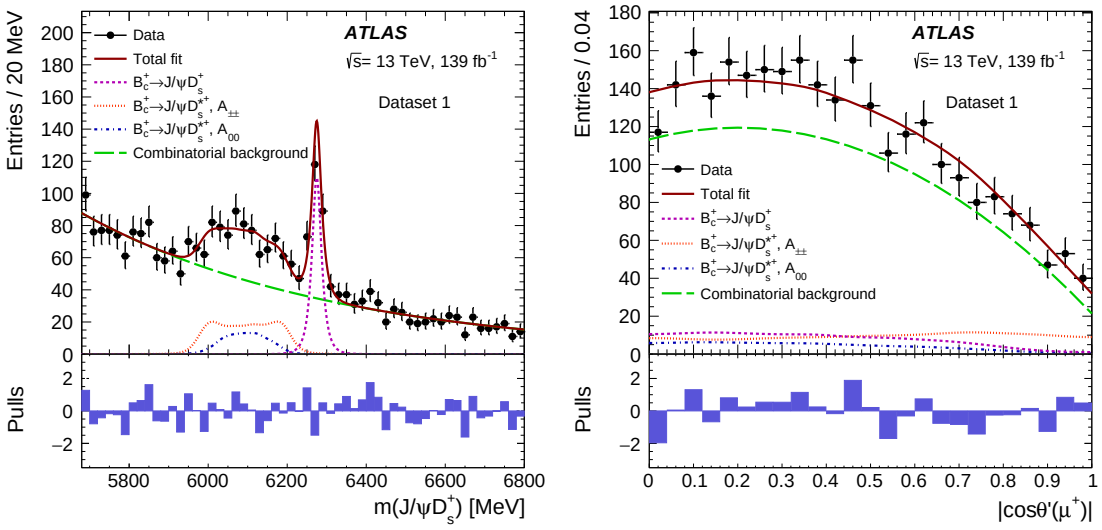

Figure 3: Fit projection to $m(J/\psi D_s^+)$ invariant mass (left) and $|\cos\theta'(\mu^+)|$ (right) distributions using Dataset 1. Taken from [9].

is a decay of pseudoscalar meson into two vector states, the final distributions can be described in terms of three helicity amplitudes: A_{--}, A_{++} and A_{00}. The analysis is performed on two non-overlapping datasets, Dataset 1 is containing events collected by the di-muon triggers or by three-muon triggers without requirements on the additional Inner Detector tracks, and Dataset 2 is using events collected only by the dedicated $B_s^0 \to \mu^+\mu^-\phi$ triggers and not by other ones used in the analysis. The extended unbinned maximum-likelihood fit to the two-dimensional distribution of $m(J/\psi D_s^+)$ and $|\cos\theta'(\mu^+)|$ is performed on both datasets simultaneously. The projection of the fit to the $J/\psi D_s^+$ invariant mass and $|\cos\theta'(\mu^+)|$ distributions using Dataset 1 is shown in Figure 3. The reference channel $B_c^+ \to J/\psi\pi^+$ is used for both decays. The ratios of the branching fractions for $J/\psi D_s^{(*)+}$ and $B_c^+ \to J/\psi\pi^+$ are found to be $R_{D_s^+/\pi^+} = 2.76 \pm 0.33(\text{stat.}) \pm 0.29(\text{syst.}) \pm 0.16(\text{ext.})$, $R_{D_s^{*+}/\pi^+} = 5.33 \pm 0.61(\text{stat.}) \pm 0.67(\text{syst.}) \pm 0.32(\text{ext.})$ and $R_{D_s^{*+}/D_s^+} = 1.93 \pm 0.24(\text{stat.}) \pm 0.09(\text{syst.})$, where the first uncertainty is statistical, the second is systematic, and the third corresponds to the external uncertainty in the branching fraction of the normalization channel. In addition to the ratios of the branching fractions, the transverse polarization fraction $\Gamma_{\pm\pm}/\Gamma$ in the $B_c^{*+} \to J/\psi D_s^{*+}$ decays were measured to be $\Gamma_{\pm\pm}/\Gamma = 0.70 \pm 0.10(\text{stat.}) \pm 0.04(\text{syst.})$. All results are compared to previous measurements by ATLAS [10] and LHCb [11] as well as to the theory predictions where the best agreement is with a QCD relativistic potential model calculation [12].

The second analysis focusing on the B_c properties is the measurement of the $B_c(2S)^+$ and $B_c^*(2S)^+$ cross-section ratios, performed by the CMS collaboration [13]. The $B_c(2S)^+$ was observed by the ATLAS experiment [14] and further analyzed by LHCb [15] and CMS [16] where the second peak, corresponding to the $B_c^*(2S)^+$, was reported. The latest result by CMS, which uses the full Run 2 data sample with an integrated luminosity of 143 fb^{-1}, aims for a precision measurement

of these decays. The $B_c^{(*)}(2S)$ is reconstructed in the $B_c^{(*)+}\pi^+\pi^-$ channel that is followed by a $B_c^+ \to J/\psi\pi^+$ decay. The soft γ from the $B_c^{*+} \to B_c^+\gamma$ is not reconstructed and for this reason, the $B_c^*(2S)^+$ peak is seen in the invariant mass distribution at a mass value lower than that of the $B_c(2S)^+$ peak as shown in Figure 4.

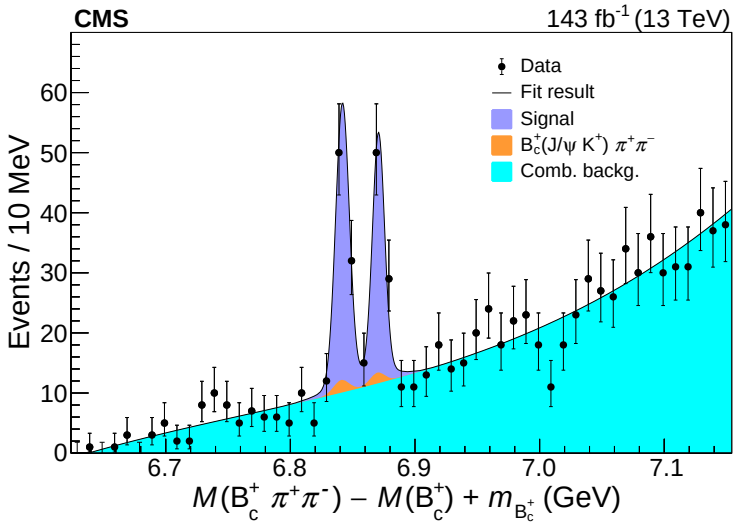

Figure 4: Invariant mass distribution of the $B_c^{(*)}(2S)^+$ candidates. The $B_c^*(2S)^+$ corresponds to the lower-mass peak, the $B_c(2S)^+$ to the higher. The fitted contributions are shown by the stacked distributions, the solid line representing their sum. Taken from [13].

An unbinned maximum likelihood fit was applied to the $\mathcal{M}(B_c^+\pi^+\pi^-) - \mathcal{M}(B_c^+) + m_{B_c^+}$ distribution, where $\mathcal{M}(B_c^+\pi^+\pi^-)$ and $\mathcal{M}(B_c^+)$ are the reconstructed invariant masses of the $B_c^+\pi^+\pi^-$ and B_c^+ candidates, respectively, and $m_{B_c^+}$ is the world-average $m_{B_c^+}$ mass [20]. This variable is used because it provides better resolution than simple $\mathcal{M}(B_c^+\pi^+\pi^-)$ distribution. The ratios of the $B_c^{(*)}(2S)^+ \to B_c^+$ and $B_c^*(2S)^+ \to B_c(2S)^+$ cross-sections, R^{*+}, R^+ and R^{*+}/R^+, were measured to be $R^+ = (3.47 \pm 0.63(\text{stat}) \pm 0.33(\text{syst}))\%$, $R^{*+} = (4.69 \pm 0.71(\text{stat}) \pm 0.56(\text{syst}))\%$ and $R^{*+}/R^+ = 1.35 \pm 0.32(\text{stat}) \pm 0.09(\text{syst})$. The behaviors of the cross-section ratios with respect to the transverse momentum p_T and rapidity were studied and revealed no significant dependence.

4. Analyses with K_s^0

Studies involving K_s^0 mesons are very challenging in the LHC environment. The $B^0 \to \psi(2S)K_s^0\pi^+\pi^-$ and $B_s^0 \to \psi(2S)K_s^0$ decays can potentially be used for CP asymmetry measurements and, in addition, the $B^0 \to \psi(2S)K_s^0\pi^+\pi^-$ can be used to search for intermediate exotic resonances. CMS performed an analysis of these decays using data from 2017 and 2018 with a total integrated luminosity of 103 fb^{-1} [17]. The $K_s^0 \to \pi^+\pi^-$ candidates are formed from displaced two-prong vertices. The $B^0 \to \psi(2S)K_s^0$ decay was chosen as the normalization channel and is fitted simultaneously with $B_s^0 \to \psi(2S)K_s^0$ decay. The invariant mass spectrum for both decay channels is shown in Figure 5.

Decays are observed with significances exceeding 5 standard deviations: $B_s^0 \to \psi(2S)K_s^0$ $\sim 5.2\sigma$ and $B^0 \to \psi(2S)K_s^0\pi^+\pi^- > 30\sigma$. The branching fraction ratio of $B_s^0 \to \psi(2S)K_s^0$ relative

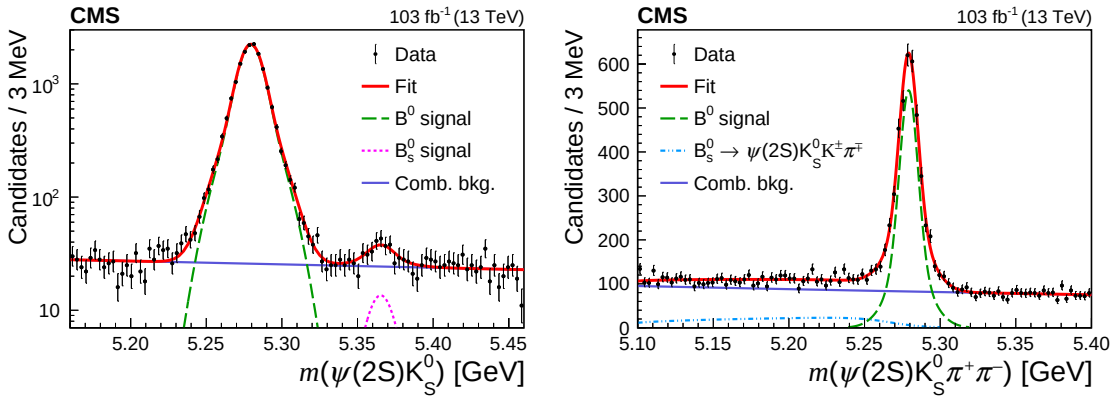

Figure 5: Measured invariant mass distributions of $\psi(2S)K^0_S$ (left) and $\psi(2S)K^0_S\pi^+\pi^-$ (right) candidates. Taken from [17].

to the $B^0 \to \psi(2S)K^0_s$ is measured to be:

$$R_s = (0.69 \pm 0.14(\text{stat.}) \pm 0.11(\text{syst.}) \pm 0.34(f_s/f_d)) \times 10^{-2},$$

where the last uncertainty is related to the used value $f_s/f_d = 0.208 \pm 0.021$. The f_s/f_d value was taken from LHCb measurement [18] and adjusted according to the B candidate transverse momentum. The branching fraction ratio of $B^0 \to \psi(2S)K^0_s\pi^+\pi^-$ relative to the $B^0 \to \psi(2S)K^0_s$ is measured to be:

$$R_{\pi^+\pi^-} = 0.480 \pm 0.013(\text{stat.}) \pm 0.032(\text{syst.}).$$

This is the first measurement of these ratios. The 2- and 3-body invariant mass distributions of the $B^0 \to \psi(2S)K^0_s\pi^+\pi^-$ decay products do not show significant exotic narrow structures in addition to the known light meson resonances. Further studies with more data will be needed to investigate more precisely the internal dynamics of the $B^0 \to \psi(2S)K^0_s\pi^+\pi^-$ decay and to perform CP asymmetry measurements in the two observed decays.

4.1 Charmonium decays

To compute amplitudes of two-body non-leptonic decays, a simple factorization method is commonly used. It has been successful; however, we know that it must be incomplete since it fails to describe the $B \to \chi_{c0}K$ mode. The $B^+ \to K^0_sK^+K^-\pi^+$ and $B^+ \to K^0_sK^+K^+\pi^-$ decays are studied since $K^0_SK\pi$ invariant mass spectra from both decay modes reveal a rich set of charmonium resonances. LHCb performed a study using the Run 1 and Run 2 datasets with combined integrated luminosity of 9 fb^{-1} focusing on the precise measurement of charmonium parameters [19].

The reconstruction of $K^0_s \to \pi^+\pi^-$ decays is divided into two categories at LHCb: the first involving K^0_s mesons that decay early enough for the pions to be reconstructed inside the VELO detector (K^0_{SLL}), and the second containing K^0_s mesons that decay later such that track segments from the pions are outside the VELO detector (K^0_{SDD}). The K^0_{SLL} has better mass, momentum, and vertex resolution, but the K^0_{SDD} has larger statistics. Both of these categories were used to reconstruct the B meson. The $K^0_SK\pi$ invariant-mass spectra were analyzed for events in the B^+

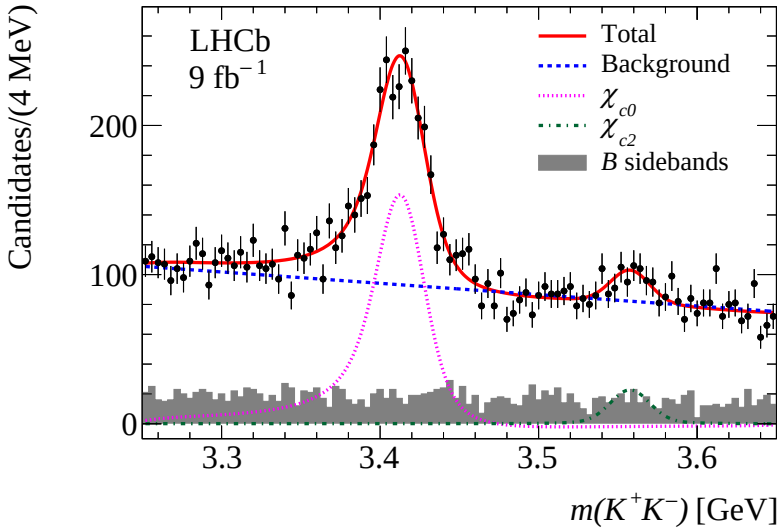

Figure 6: Invariant K^+K^- mass distribution in the $\chi_{c0} - \chi_{c2}$ mass region for $B \to K^0_S K^+K^-\pi^+$ decays. Taken from [19].

signal region, summed over the K^0_{SLL} and K^0_{SDD} datasets. The $K^0_S K\pi$ invariant spectrum mass contains a broad distribution of resonances, such as the η_c, J/ψ, χ_{c1} and $\eta_c(2S)$.

The measurements of charmonium-resonance parameters such as mass, width and branching ratio were performed with binned fits to the $K^0_S K\pi$ invariant-mass spectra separately in the range of (2.90 – 3.15) GeV for $\eta_c - J/\psi$ mass region and the range of (3.46 – 3.70) GeV for $\chi_{c1} - \eta_c(2S)$ mass region. The K^+K^- invariant mass spectrum from the $B \to K^0_s K^+K^-\pi^+$ decays is also analyzed. The invariant mass region between 3.2 GeV and 3.7 GeV shows two additional charmonium resonances for $B^+ \to \chi_{c0}K^0_S\pi^+$ and $B^+ \to \chi_{c2}K^0_S\pi^+$, as shown in Figure 6. The branching fractions of these two decays were measured with respect to two normalization resonances η_c and J/ψ as shown in Table 1. This is the first measurement of the branching fraction of $B^+ \to \chi_{c0}K^0_S\pi^+$. For the $B^+ \to \chi_{c2}K^0_S\pi^+$ branching fraction, the tension of 2.6σ (3.2σ) using the η_c (J/ψ) meson as a reference, is found with respect to the PDG value [20].

Final state	$\mathcal{B}_\infty$ ($\times 10^{-3}$)	PDG ($\times 10^{-3}$)
$B^+ \to \chi_{c0}K^0\pi^+$	$1.38 \pm 0.07 \pm 0.11 \pm 0.32$	
$B^+ \to \chi_{c2}K^0\pi^+$	$0.87 \pm 0.20 \pm 0.08 \pm 0.20$	0.116 ± 0.025
Final state	$\mathcal{B}_\in$ ($\times 10^{-3}$)	
$B^+ \to \chi_{c0}K^0\pi^+$	$1.45 \pm 0.08 \pm 0.11 \pm 0.16$	
$B^+ \to \chi_{c2}K^0\pi^+$	$0.92 \pm 0.21 \pm 0.08 \pm 0.10$	

Table 1: Measured branching fractions using (top) the η_c and (bottom) the J/ψ resonance as the reference for $B^+ \to K^0K^+K^-\pi^+$ data. The first uncertainty is statistical, the second systematic, the third due to the PDG [20] uncertainty on the $B^+ \to \eta_c K^+$ or $B^+ \to J/\psi K^+$ branching fraction. The PDG reports an upper limit $\mathcal{B}(B^+ \to \chi^0_c K^{*+}) < 0.21 \times 10^{-3}$. Taken from [19].

5. Excited Ξ_b baryon search

The Ξ baryon family consists of isodoublet states composed of bsq quarks, where q represents an up or a down quark. Various theoretical models and calculations predict a spectrum of excited Ξ_b baryons. Three of the four excited states with di-quark angular momentum $j_{qs} = 1$ were observed in $\Xi_b^-\pi^+$ and $\Xi_b^0\pi^-$ decays. CMS focused on the search for the Ξ_b^- excited states in the $\Xi_b^-\pi^+\pi^-$ invariant mass spectrum using full Run 2 a dataset with an integrated luminosity of 140 fb^{-1} [21]. The ground state Ξ_b is reconstructed via its decays to $J/\psi\Xi^-$ and $J/\psi\Lambda K^-$, followed by the decays $\Xi^- \to \Lambda\pi^-$ and $\Lambda \to p\pi^-$. Partially reconstructed $\Xi_b^- \to J/\psi\Sigma^0 K^-$ events, where the photon from the $\Sigma^0 \to \Lambda\gamma$ decay is too soft to be detected, were included in the $J/\psi\Lambda K^-$ invariant mass spectrum with the shape parameters fixed from simulation studies as shown in Figure 7.

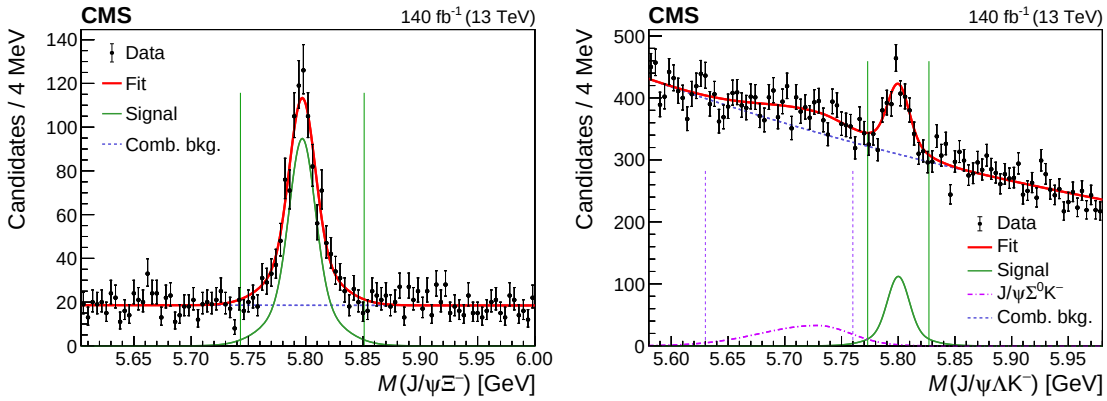

Figure 7: Invariant mass distribution of the selected Ξ_b^- candidates in the $J/\psi\Xi^-$ (left) and $J/\psi\Lambda K^-$ (right) decay channels with the fit results superimposed. Taken from [21].

The $\Xi_b^-\pi^+\pi^-$ candidates are formed by combining the selected Ξ_b^- candidates with two opposite side tracks originating from the same primary vertex. Since the resolutions in the $J/\psi\Xi^-$ and $J/\psi\Lambda K^-$ channels are similar, both signal regions, defined around Ξ_b^- peaks, were analyzed simultaneously. The partially reconstructed events using Ξ_b^- candidates in the $5.63 < M(J/\psi\Lambda K^-) < 5.76$ GeV mass region were analyzed separately. Independent unbinned extended maximum-likelihood fits were applied to the mass difference variable ΔM for both the signal and the partially reconstructed regions. The model projections for the mass difference variable using the signal region of the Ξ_b resonance is shown in Figure 8. A new resonance was observed with $\Delta M_{\Xi_b(6100)^-} = (24.14 \pm 0.22)$ MeV, where the uncertainty is statistical only. An upper limit on the width $\Gamma(\Xi_b(6100)^-) < 1.9$ MeV has been obtained through a scan of the profiled likelihood, assuming an asymptotic distribution. The local significance is evaluated with the likelihood ratio technique, and the result varies between 6.2σ and 6.7σ using the signal and partially reconstructed regions, respectively. The known Ξ_b^- mass of 5797.0 ± 0.6 MeV is used to obtain $M(\Xi_b(6100)^-) = 6100.3 \pm 0.2(\text{stat}) \pm 0.1(\text{syst}) \pm 0.6(\Xi_b^-)$ MeV. The new $\Xi_b(6100)^-$ resonance and its decay sequence are consistent with the lightest orbitally excited Ξ_b^- baryon, with the $j_{ds} = 1$ and $J^P = 3/2^-$. The observation of this baryon and the measurement of its properties provide information that can help to distinguish between different theoretical models used to calculate the properties of the excited Ξ_b states.

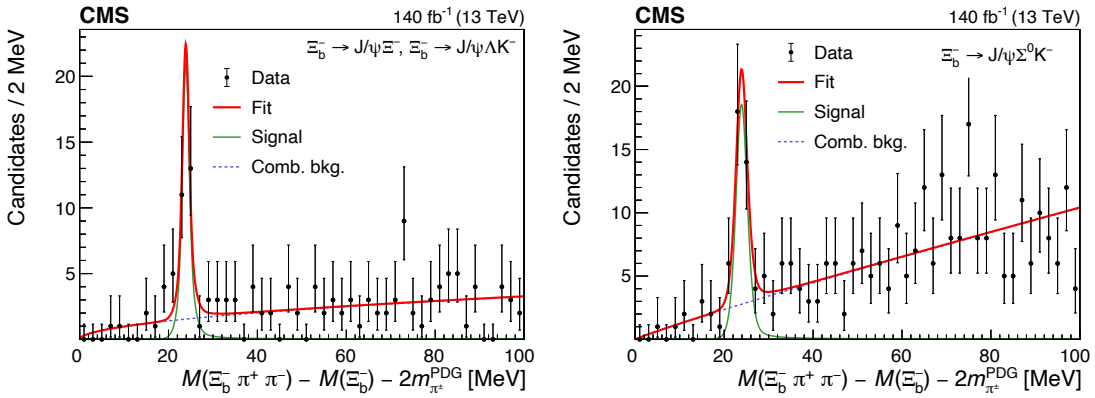

Figure 8: Distribution of the invariant mass difference ΔM for the selected $\Xi_b^-\pi^+\pi^-$ candidates, with the Ξ_b^- reconstructed in the $J/\psi\Xi^-$ and $J/\psi\Lambda K^-$ channels (left) and partially reconstructed in the $\Xi_b^- \to J/\psi\Sigma^0 K^-$ channel (right). Taken from [21].

6. Open-charm measurements

Cross-section measurements of open-charm mesons are an important test of QCD. CMS studied the cross-sections for the prompt production of D^{*+}, D^0, and D^+ mesons using 29 nb^{-1} of pp collisions at 13 TeV collected in year 2016 [22]. The events were collected with an unbiased trigger that required only the presence of crossing beams to avoid any bias from a trigger requirement that would aim to select events and require an efficiency correction. The charm mesons are identified via their exclusive decays:

- $pp \to D^{*+}X \to D^0\pi_s^+X \to K^-\pi^+\pi_s^+X$,
- $pp \to D^0X \to K^-\pi^+X$,
- $pp \to D^+X \to K^-\pi^+\pi^+X$,

where X corresponds to any set of possible particles and π_s^+ denotes a "slow" pion that has significantly lower momentum than the kaon and pion decay products of the D^0.

The mass distributions were fitted in bins of D meson p_T and rapidity for the $\Delta M = M(K^-\pi^+\pi_s^+) - M(K^-\pi^+)$, $M(K\pi)$ and $M(K\pi\pi)$ distributions in the kinematic range $4 < p_\text{T} < 100$ GeV and $|\eta| < 2.1$. Measured production cross-sections were compared with theoretical predictions using the FONLL [23, 24] and various PYTHIA models [25, 26]. An example of differential cross-sections for prompt $D^*(2010)^\pm$ meson production is shown in Figure 9. Overall, the best description is obtained by the upper edge of the FONLL uncertainty band. The agreement with the different predictions is fair in the wide kinematic range analyzed, but no single Monte Carlo simulation or theoretical prediction describes the data well over the entire kinematic range. The cross-sections were also compared with measurements from ATLAS, ALICE and LHCb and with $PbPb$ data measured by CMS. None of them cover the same kinematic region at the same center-of-mass energy, however; it is useful to see the consistency in combination with the FONLL predictions.

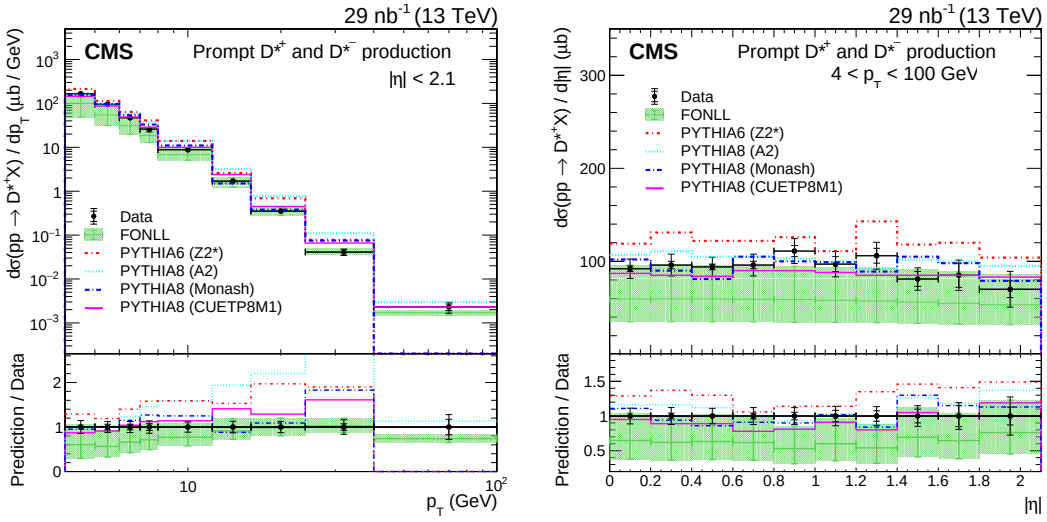

Figure 9: Differential cross-sections $d\sigma/dp_{\mathrm{T}}$ (upper) and $d\sigma/d|\eta|$ (lower) for prompt $D^*(2010)^{\pm}$ meson production. Taken from [22].

7. Summary

An overview of recent non-leptonic hadron decays measurements at LHC was presented. The spectrum of research activities in this field at the LHC experiments is very wide. With a large sample of LHC data at $\sqrt{s}$ = 13 TeV, rare processes are experimentally accessible. The main goal is to understand the production dynamics of the hadronic decays and to precisely describe their parameters. Any new results in this field help to improve existing theoretical models that could lead to discoveries.

Acknowledgments

I acknowledge support from the National Science Foundation grant number 1906674.

References

[1] L. Evans and P. Bryant, "LHC Machine," JINST **3** (2008), S08001

[2] G. Aad *et al.* [ATLAS], "The ATLAS Experiment at the CERN Large Hadron Collider," JINST **3** (2008), S08003

[3] S. Chatrchyan *et al.* [CMS], "The CMS Experiment at the CERN LHC," JINST **3** (2008), S08004

[4] A. A. Alves, Jr. *et al.* [LHCb], "The LHCb Detector at the LHC," JINST **3** (2008), S08005

[5] LHCb collaboration, "Search for the rare hadronic decay $B_s^0 \to p\bar{p}$," [arXiv:2206.06673 [hep-ex]].

[6] Y. K. Hsiao, S. Y. Tsai, C. C. Lih and E. Rodrigues, "Testing the W-exchange mechanism with two-body baryonic B decays," JHEP **04** (2020), 035 [arXiv:1906.01805 [hep-ph]].

[7] S. S. Wilks, "The Large-Sample Distribution of the Likelihood Ratio for Testing Composite Hypotheses," Annals Math. Statist. **9** (1938) no.1, 60-62

[8] LHCb collaboration, "Searches for the rare hadronic decays $B^0 \to p\bar{p}p\bar{p}$ and $B_s^0 \to p\bar{p}p\bar{p}$," [arXiv:2211.08847 [hep-ex]].

[9] G. Aad *et al.* [ATLAS], "Study of $B_c^+ \to J/\psi D_s^+$ and $B_c^+ \to J/\psi D_s^{*+}$ decays in pp collisions at $\sqrt{s}$ = 13 TeV with the ATLAS detector," JHEP **08** (2022), 087 [arXiv:2203.01808 [hep-ex]].

[10] G. Aad *et al.* [ATLAS], "Study of the $B_c^+ \to J/\psi D_s^+$ and $B_c^+ \to J/\psi D_s^{*+}$ decays with the ATLAS detector," Eur. Phys. J. C **76** (2016) no.1, 4 [arXiv:1507.07099 [hep-ex]].

[11] R. Aaij *et al.* [LHCb], "Observation of $B_c^+ \to J/\psi D_s^+$ and $B_c^+ \to J/\psi D_s^{*+}$ decays," Phys. Rev. D **87** (2013) no.11, 112012 [arXiv:1304.4530 [hep-ex]].

[12] P. Colangelo and F. De Fazio, "Using heavy quark spin symmetry in semileptonic B_c decays," Phys. Rev. D **61** (2000), 034012 [arXiv:hep-ph/9909423 [hep-ph]].

[13] A. M. Sirunyan *et al.* [CMS], "Measurement of $B_c(2S)^+$ and $B_c^*(2S)^+$ cross section ratios in proton-proton collisions at $\sqrt{s}$ = 13 TeV," Phys. Rev. D **102** (2020) no.9, 092007 [arXiv:2008.08629 [hep-ex]].

[14] G. Aad *et al.* [ATLAS], "Observation of an Excited $B_c^\pm$ Meson State with the ATLAS Detector," Phys. Rev. Lett. **113** (2014) no.21, 212004 [arXiv:1407.1032 [hep-ex]].

[15] R. Aaij *et al.* [LHCb], "Observation of an excited B_c^+ state," Phys. Rev. Lett. **122** (2019) no.23, 232001 [arXiv:1904.00081 [hep-ex]].

[16] A. M. Sirunyan *et al.* [CMS], "Observation of Two Excited B_c^+ States and Measurement of the $B_c^+(2S)$ Mass in pp Collisions at $\sqrt{s}$ = 13 TeV," Phys. Rev. Lett. **122** (2019) no.13, 132001 [arXiv:1902.00571 [hep-ex]].

[17] A. Tumasyan *et al.* [CMS], "Observation of $B^0 \to \psi(2S) K_S^0 \pi^+\pi^-$ and $B_S^0 \to \psi(2S) K_S^0$ decays," Eur. Phys. J. C **82** (2022), 499 [arXiv:2201.09131 [hep-ex]].

[18] R. Aaij *et al.* [LHCb], "Precise measurement of the f_s/f_d ratio of fragmentation fractions and of B_s^0 decay branching fractions," Phys. Rev. D **104** (2021) no.3, 032005 [arXiv:2103.06810 [hep-ex]].

[19] R. Aaij *et al.* [LHCb], "Study of charmonium decays to $K_S^0 K\pi$ in the $B \to (K_S^0 K\pi)K$ channels," [arXiv:2304.14891 [hep-ex]].

[20] R. L. Workman *et al.* [Particle Data Group], "Review of Particle Physics," PTEP **2022** (2022), 083C01

[21] A. M. Sirunyan *et al.* [CMS], "Observation of a New Excited Beauty Strange Baryon Decaying to $\Xi_b^- \pi^+ \pi^-$," Phys. Rev. Lett. **126** (2021) no.25, 252003 [arXiv:2102.04524 [hep-ex]].

[22] A. Tumasyan *et al.* [CMS], "Measurement of prompt open-charm production cross sections in proton-proton collisions at $\sqrt{s}$ = 13 TeV," JHEP **11** (2021), 225 [arXiv:2107.01476 [hep-ex]].

[23] M. Cacciari, M. Greco and P. Nason, "The p_T spectrum in heavy flavor hadroproduction," JHEP **05** (1998), 007 [arXiv:hep-ph/9803400 [hep-ph]].

[24] M. Cacciari, M. L. Mangano and P. Nason, "Gluon PDF constraints from the ratio of forward heavy-quark production at the LHC at $\sqrt{s}$ = 7 and 13 TeV," Eur. Phys. J. C **75** (2015) no.12, 610 [arXiv:1507.06197 [hep-ph]].

[25] T. Sjöstrand, S. Mrenna and P. Z. Skands, "PYTHIA 6.4 Physics and Manual," JHEP **05** (2006), 026 [arXiv:hep-ph/0603175 [hep-ph]].

[26] T. Sjöstrand, S. Ask, J. R. Christiansen, R. Corke, N. Desai, P. Ilten, S. Mrenna, S. Prestel, C. O. Rasmussen and P. Z. Skands, "An introduction to PYTHIA 8.2," Comput. Phys. Commun. **191** (2015), 159-177 [arXiv:1410.3012 [hep-ph]].